

---

**The relationship between the North Atlantic jet and tropical  
convection over the Indian and western Pacific Oceans**

JIACAN YUAN<sup>1</sup> \*; STEVEN B. FELDSTEIN<sup>2</sup>, SUKYOUNG LEE<sup>2</sup>,  
AND BENKUI TAN<sup>1</sup>

<sup>1</sup>*Department of Atmospheric and Oceanic Sciences, Peking University, Beijing, China*

<sup>2</sup>*Department of Meteorology, The Pennsylvania State University, University Park, Pennsylvania*

*Journal of Climate*

---

\* *Corresponding author address:* Jiacan Yuan, Department of Atmospheric and Oceanic Sciences, School of Physics, Peking University, Beijing 100871, China

E-mail: [jiacan.yuan@gmail.com](mailto:jiacan.yuan@gmail.com)

## ABSTRACT

Boreal winter jet variability over the North Atlantic is investigated using ERA-40 re-analysis data, where the variability is defined by the first EOF of the zonal wind on seven vertical levels. The principal component time series of this EOF is referred to as the jet index. A pattern correlation analysis indicates that the jet index more accurately describes intraseasonal North Atlantic zonal wind variability than does the NAO.

A series of composite calculations of the jet index based on events of intraseasonal convective precipitation over the tropical Indian and western Pacific Oceans reveals the following statistically significant relationships: (1) negative jet events lead enhanced Indian Ocean precipitation; (2) positive jet events lag enhanced Indian Ocean precipitation; (3) positive jet events lead enhanced western Pacific Ocean precipitation; (4) negative jet events lag enhanced western Pacific Ocean precipitation; These intraseasonal relationships are found to be linked through the circumglobal teleconnection pattern (CTP). Implications of the sign of the CTP being opposite to that of the jet index suggest that relationships (1) and (3) may arise from cold air surges associated with the CTP over these oceans. On interdecadal time scales, a much greater increase in the frequency of precipitation events from 1958-1979 (P1) to 1980-2001 (P2) was found for the Indian Ocean relative to the western Pacific Ocean. This observation, combined with relationships (2) and (4), leads to the suggestion that this change in the frequency of intraseasonal Indian Ocean precipitation events may make an important contribution to excitation of interdecadal variability of the North Atlantic jet.

# 1. Introduction

The North Atlantic Oscillation (NAO) (Lorenz and Hartmann 2003; Wittman et al. 2005; Woollings et al. 2010), which is the dominant teleconnection pattern of the Northern Hemisphere (NH), is characterized by north-south meanders of the eddy-driven jet (e.g., Eichelberger and Hartmann 2007; Athanasiadis and Wallace 2010; Woollings et al. 2010). The NAO has been shown to exhibit variability on all time scales, from its intrinsic time scale of about 10 days (Feldstein 2000), to decades (e.g., Hurrell and Loon 1997), and even centuries (e.g., Semenov et al. 2008). Insight into the mechanisms that drive the interdecadal variability of the NAO was obtained by the atmospheric general circulation model experiments of Hoerling et al. (2001). They found that a warming of the Indian and Pacific Ocean surfaces was able to force a circulation pattern over the North Atlantic that resembles the observed trend pattern for the latter half of the 20th century, which is very similar to the positive phase of the NAO. In the same vein, later studies have also suggested that a warming of the tropical Indian Ocean surface is associated with the positive polarity of the NAO (Hoerling et al. 2004; Selten et al. 2004; Bader and Latif 2005; Zhou and Miller 2005; Li et al. 2006). These findings contrast with those of Cohen and Barlow (2005) who argued that the sea surface temperature (SST) trend in the Indo-western Pacific warm pool region is unrelated with the NAO trend.

On intraseasonal time scales, there is also evidence that tropical convection can modify the wintertime circulation over the North Atlantic. For example, phase 3 of the tropical Madden-Julian Oscillation (MJO) index of Wheeler and Hendon (2004), which is characterized by enhanced convection over the Indian Ocean, and reduced convection over the western

Pacific Ocean, is associated with the positive polarity of the Arctic Oscillation (AO)/NAO (Zhou and Miller 2005; Cassou 2008; L'Heureux and Higgins 2007; Lin et al. 2009; Lin and Brunet 2011). When the MJO is observed to be in phase 6, which exhibits opposite convection characteristics to that of phase 3, the AO/NAO indices tend to coincide with their negative polarity. While processes internal to extratropical dynamics can generate north-south jet meanders (Robinson 1993; Lee and Feldstein 1996; Yu and Hartmann 1993), the above studies suggest that North Atlantic jet variability, over a very broad range of time scales, may be influenced by convection over the tropical Indian and western Pacific Oceans.

As was emphasized by Palmer (1988), the tie between tropical convection and the extratropical circulation does not necessarily mean that the latter is slaved to the former. In their examination of an MJO event during the boreal winter of 1985-1986, Hsu et al. (1990) found that a subtropical Rossby wave train, propagating southeastward from the North Atlantic to the Indian Ocean, may have triggered convection over the Indian Ocean. Similar high-frequency Rossby wave trains were also observed to propagate southeastward from the Asian-Pacific jet and force convection over the central tropical Pacific (Matthews and Kiladis 1999; Palmer 1988). Matthews (2008) concluded that subtropical Rossby wave activity, associated with the African-Asian jet, can organize some of the MJO events. With a numerical model, Lin and Brunet (2011) found that there is a strong NH extratropical influence on the MJO, with significant forecast skill at 10 to 25 day lead times.

Bader and Latif (2005) suggested that tropical Indian Ocean convection and the NAO may be linked through the circumglobal teleconnection pattern (CTP), which is defined as first two empirical orthogonal functions (EOFs) of the monthly-mean 300-hPa nondivergent meridional wind field Branstator (2002). (As discussed in Branstator 2002, the CTP is a

zonal wavenumber 5 pattern that spans all longitudes across the globe. Because this pattern can take on any longitudinal phase, it must be represented by two EOFs.) They argued that the CTP plays a key role in the formation of a NAO-like pattern through its carrying wave like perturbations from southern Asia toward the North Atlantic. Selten et al. (2004) found with CCM3 simulations that in response to enhanced greenhouse gas concentration, precipitation over the tropical western Pacific intensifies and the trend pattern takes on the form of the CTP. In another study, based on their analysis of the propagation characteristics of circumglobal wave packets, Feldstein and Dayan (2008) suggested that the CTP can be interpreted as corresponding to a time-average of an eastward propagating wave packet that has a phase speed which is close to zero. It is this near zero phase speed which can account for the occurrence of the CTP in data that is averaged over time periods greater than one month (Watanabe 2004).

Motivated by the above findings, the goal of this study is to investigate (1) to what extent the NAO can capture the actual north-south meanders of the North Atlantic jet (hereafter referred to simply as *jet* in most places); (2) on intraseasonal time scales, whether there is a link between jet variability and tropical convection over the Indian and western Pacific Oceans, respectively; (3) whether and to what extent the CTP is involved in the intraseasonal jet variability; (4) on interdecadal time scales, whether the jet has exhibited a trend during the latter part of the 20th century; if so, (5) whether this interdecadal trend can be explained in terms of changes in the intraseasonal variability of convection over the tropical Indian and western Pacific Oceans.

The approach to be adopted in this study will be mostly qualitative, focusing on determining the lag/lead relationships between tropical convection, the CTP, and the jet variability

on intraseasonal time scales, and then using these results to better evaluate interdecadal trends. For future research, we plan to use idealized numerical models to quantitatively investigate the dynamical mechanisms that drive these relationships.

The data and methodology are presented in Section 2. Circulation patterns associated with intraseasonal jet variability are shown in Section 3. Section 4 presents an analysis of the CTP signal associated with the jet variability. In Section 5, we examine the relationship on intraseasonal time scales between tropical convective heating over the Indian and western Pacific Oceans and the North Atlantic jet. Section 6 discusses how interdecadal variability of the North Atlantic jet may be related to changes in the frequency of occurrence of intraseasonal tropical convection. The discussion and conclusions are given in section 7.

## 2. Data and methodology

This study uses European Centre for Medium-Range Weather Forecasts (ECMWF) ERA-40 reanalysis data (Uppala et al. 2005) for the period of 1958 to 2002. Because our focus is on the boreal winter, data for the months of December, January and February (DJF) are analyzed. The main variables to be analyzed are 250-hPa zonal wind and streamfunction, and convective precipitation. The latter variable is used as a proxy for convective heating. Although there are quality issues associated with the ERA-40 tropical precipitation data (Uppala et al. 2005), as we will show in Fig. 6, the relationship between the tropical precipitation and jet variability in the ERA-40 data is similar with that seen with the Climate-Prediction-Center Merged Analysis of Precipitation (CMAP) dataset (Figs. 6b and c).

*a. Construction of and comparison between the North Atlantic jet variability and NAO indices*

Jet variability is identified by performing Empirical Orthogonal Function (EOF) analysis on the 1958-2002 DJF zonal wind field where the analysis domain spans  $50^{\circ}\text{W}$ - $20^{\circ}\text{E}$ ,  $10^{\circ}\text{N}$ - $80^{\circ}\text{N}$ , over seven vertical levels: 100, 150, 200, 250, 300, 400, 500hPa. Prior to this calculation, the seasonal cycle is removed from the daily data. The first EOF (Fig. 1a), which explains 18.6% of the variance, has two positive centers near  $20^{\circ}\text{N}$  and  $60^{\circ}\text{N}$ , with a negative center near  $40^{\circ}\text{N}$ . (The western boundary of the EOF analysis was chosen to include the North Atlantic subtropical jet. An EOF analysis with the western domain boundary extended to  $70^{\circ}\text{W}$  exhibited little change in spatial structure (not shown), with the corresponding principal component time series having a linear correlation of 0.95.) Since the time-mean flow over the North Atlantic is comprised of two jets (not shown), a subtropical jet and an eddy-driven jet, the positive jet phase corresponds to these two jets becoming more distinct, and the negative jet phase to a merging of these two jets into a single jet centered at  $40^{\circ}\text{N}$ . Figure 1b shows that the center near  $60^{\circ}\text{N}$  has a deeper vertical structure than that near  $20^{\circ}\text{N}$ , consistent with the former (latter) being associated with an eddy-driven (subtropical) jet.

In order to examine the extent to which EOF1 actually occurs in the atmosphere, a pattern correlation was calculated between EOF1 and the daily zonal wind field. The calculation was performed for both positive and negative jet polarities. The pattern correlation is computed following

$$Corr(t) = \frac{\sum_k \sum_i \sum_j EOF1(i, j, k)U(i, j, k, t)}{(\sum_k \sum_i \sum_j EOF1^2(i, j, k))^{1/2}(\sum_k \sum_i \sum_j U^2(i, j, k, t))^{1/2}} \quad (1)$$

where EOF1 is the spatial pattern of the leading mode, and U is the zonal wind for those days when the jet index is above (below) one standard deviation for the positive (negative) phase. The indices  $i$ ,  $j$ , and  $k$  correspond to grid points in the zonal, meridional, and vertical directions, respectively, and  $t$  is time. To quantify the extent to which EOF1 corresponds to the observed zonal wind field, a histogram was constructed by counting the number of days for which the pattern correlations fall into bins with an interval of 0.05. The number of days counted for each bin is then divided by the total number of days to yield a percentage. The resulting histograms are shown in Figs. 2a and 2b for the positive and negative phases, respectively. It is found that 76% of the positive-phase days have a pattern correlation that is greater than 0.6, with a median value of 0.67. For the negative phase, 88% of the days have a pattern correlation that exceeds 0.6, with a median value of 0.75.

Because the NAO is commonly used to represent variability over the North Atlantic during the winter (van Loon and Rogers 1978; Wallace and Gutzler 1981; Hurrell 1995), to examine whether the NAO is better than the jet index in describing the variability of the North Atlantic jet, we repeated the pattern correlation calculation for the NAO. For this purpose, we use the NAO index provided by the Climate Prediction Center (CPC; [http://www.cpc.noaa.gov/products/precip/CWlink/pna/nao\\_index.html](http://www.cpc.noaa.gov/products/precip/CWlink/pna/nao_index.html)), where the NAO pattern is defined as the first rotated EOF of monthly mean 500-hPa geopotential height over the North Atlantic during the 1950-2000 period. We approximated the spatial structure of the NAO by calculating a composite of the monthly mean 500-hPa geopotential height based

on the NAO index from the CPC. (A daily CPC NAO index was generated by projecting the daily 500-hPa height field onto the NAO spatial pattern. For the overlapping period of 1958-2000, the correlation between the CPC's daily NAO index and our jet index is found to be 0.48.) Daily pattern correlations were then calculated between this CPC-NAO pattern and the daily 500-hPa geopotential height field, over the domain of 50°W-20°E and 10°N-80°N, for those days when the amplitude of the NAO index exceeds one standard deviation. The resulting histograms are shown in Figs. 2c and 2d. Compared with Figs. 2a and 2b, the distributions are concentrated at lower values, with a median correlation of 0.52 for the positive phase and 0.48 for the negative phase. For a more direct comparison with the jet index, we also constructed a 250-hPa zonal wind field associated with the NAO. This zonal wind field was obtained in the same manner as that for the NAO geopotential height. The resulting histograms for the zonal wind field are shown in Fig. 2e for the positive phase, which has a median value of 0.23, and in Fig. 2f for the negative phase, which shows a median value of 0.29.

The above pattern correlations indicate that the jet index more accurately characterizes the actual zonal wind variability over the North Atlantic than does the NAO index. Therefore, for the rest of the paper, the jet index will be utilized to investigate North Atlantic jet variability.

### *b. Selection criteria of the jet events*

To identify jet events, we first note that the e-folding time scale for the index is found to be 6 days. Therefore, to examine the evolution of the circulation patterns associated

with the jet index, composite jet events will be examined using daily data. Furthermore, the interannual variability is removed by subtracting the DJF mean value for each winter from the daily data. We select both positive and negative events following the criteria of Benedict et al. (2004). First, if four or more consecutive days have jet index values greater than one standard deviation, this set of consecutive days is chosen as a ‘candidate’. Next, for this candidate, the ‘lag-0 day’ is defined as the day on which the jet index reaches its peak. We designate the period spanning from lag -15 days to lag +15 days as an event. Finally, events are discarded if the jet index does not grow monotonically for negative lags and decay monotonically for positive lags. This selection procedure yielded 42 positive and 42 negative events during the winter season from 1958 to 2002.

*c. CTP index*

To investigate the CTP, and its relationship to tropical convection and jet variability, this study uses daily circumglobal wave packet (Feldstein and Dayan 2008) indices which are available at <http://www.meteo.psu.edu/~sbf1/>. These indices are based on the first two EOFs of the monthly mean 300-hPa nondivergent meridional wind, which define the CTP (Branstator 2002). As shown in Figs. 3a and 3b, the first two EOF spatial patterns have 10 extrema: 5 positive and 5 negative. Centered at each of these extrema, the daily 300-hPa meridional wind fields were projected onto the EOF spatial pattern, confined to a domain that extends from 90 degrees longitude upstream to 90 degrees downstream of the extremum. In this manner, for each of the two EOFs, 10 projection time series are generated. Since these projections are confined longitudinally, composites based on these indices yield

spatial patterns that resemble localized wave packets. As such, the CTP indices can be interpreted as corresponding to the amplitude of the local wave packets that comprise the CTP, as discussed in the introduction.

*d. Convective precipitation indices*

To investigate the relationship between North Atlantic jet variability and convection over the tropical Indian and western Pacific Oceans, we define two sets of convective precipitation indices. Our aim is first to focus on the intraseasonal time scale features of the tropical convection/North Atlantic jet relationship, followed by a brief investigation of how this intraseasonal time scale relationship can impact interdecadal jet variability. For this purpose, our convective precipitation indices will be defined in a manner which combines features of both intraseasonal and interdecadal variability in tropical convection. With regard to the interdecadal time scales, the Indian Ocean SST has been shown to be associated with the positive NAO (Hoerling et al. 2004), while western Pacific SST is linked to the negative NAO (Selten et al. 2004). Therefore, one convective precipitation index is defined for the Indian Ocean, and the other for the western Pacific Ocean. The former is obtained by averaging the convective precipitation over the domain covering  $20^{\circ}\text{S}$ - $10^{\circ}\text{N}$  and  $50^{\circ}\text{E}$ - $110^{\circ}\text{E}$ , and the latter by averaging over the domain of  $20^{\circ}\text{S}$ - $10^{\circ}\text{N}$  and  $120^{\circ}\text{E}$ - $180^{\circ}\text{E}$ . To account for intraseasonal variability of the convective precipitation within these two domains, daily, unfiltered convective precipitation data is used. Our motivation for using daily, unfiltered data is that the jet index has a 6-day e-folding time scale, as discussed above, and as we will find, the convective precipitation indices defined in this manner will also fluctuate over

a time period of several days. For these indices, both the seasonal cycle and the interannual variability are subtracted.

To separate the circulation pattern associated with convective heating over the Indian Ocean from that over the western Pacific Ocean, a second set of indices is defined which is based on those days when the western Pacific precipitation index is large and the Indian Ocean precipitation index is close to zero, and vice versa. More specifically, the exclusive western Pacific precipitation (WP) index is constructed by projecting the daily convective precipitation onto the composite convective precipitation pattern which is based on those days when the western Pacific precipitation index is larger than one standard deviation and the Indian Ocean precipitation index less than 0.3 standard deviations. The exclusive Indian Ocean precipitation (IO) index is obtained in an analogous manner. The projection time series are written as

$$P(t) = \frac{\sum_j \sum_i CP(i, j, t) CP_S(i, j) \cos\theta}{\sum_j \sum_i CP_S^2(i, j) \cos\theta} \quad (2)$$

where  $CP(i, j, t)$  is the daily convective precipitation field, and  $CP_S(i, j)$  is the composite spatial pattern.

With the exception of the precipitation composites, the statistical significance of all composites is obtained with the Student's  $t$ -test. For the convective precipitation, because its distribution does not follow Gaussian form, we adopt a Monte Carlo approach to evaluate statistical significance. For this purpose, for the 1958–2002 time period, 1000 composite convective precipitation fields were generated, with each composite being composed of  $N$  randomly selected days, where  $N$  corresponds to the number of WP or IO events. The resulting distribution of convective precipitation values was then used to determine the 95%

significance level at each grid point.

### **3. Intraseasonal characteristics of the 250-hPa streamfunction**

To examine the intraseasonal evolution of the circulation anomalies associated with the jet events, the approach we use here is to calculate lagged composites of 250-hPa streamfunction for both jet phases. Figure 4 shows the composite evolution of the 250-hPa streamfunction field. On the lag 0 day, for the positive jet phase, there are two centers of enhanced westerlies over the North Atlantic, at 20°N and at 60°N. This pattern is consistent with the EOF1 spatial structure (Fig. 1). Consistently, for the negative jet phase, enhanced westerlies centered at 40°N are observed. For both phases and for both positive and negative lags, hints of west-east oriented wave trains can be seen. For the positive phase, a wave train with statistically significant anomalies is observed across Asia and into the northwestern Pacific Ocean at positive lags (Figs. 4e and 4f). Similarly, for the negative phase, at lag +5 days (Fig. 4k), a statistically significant wave train propagates southeastward through North Africa and the Middle East, together with a second wave train that extends across southern Asia (including an anticyclone over the Indian subcontinent) and the northwestern Pacific. This feature over Asia is reminiscent of the wave pattern that occurred on January 3 1986, described in Hsu et al. (1990). They showed that waves originating from the extratropics can excite convection over the tropical Indian Ocean. Palmer (1988) showed that extratropical waves can also excite convection over the western Pacific Ocean. The relationship between

these wave trains and tropical convection will be examined more quantitatively with the CTP indices in section 5.

For the negative lags of the jet index, the most notable feature observed in the negative jet phase is a statistically significant wave train pattern over the North Pacific and North America at lag -9 days (Fig. 4h) and a Pacific-North America (PNA)-like wave pattern at lag -5 days (Fig. 4i). For the positive jet phase, similar wave patterns are not apparent at negative lags.

## **4. Circumglobal teleconnection pattern: Intraseasonal variability**

In the previous section, we observed the presence of wave trains at both positive and negative lags (Fig. 4). These wave trains showed features that are reminiscent of the CTP (Fig. 3) of Branstator (2002) and Feldstein and Dayan (2008). To quantitatively examine the extent to which the CTP is associated with jet variability, we performed lagged composites of the CTP indices relative to the jet index described in Section 2. Again, the interannual variability is removed. As described in subsection 2c, the numbers that correspond to the 10 extrema in Figs. 3a and 3b denote the CTP indices. They mark the center of the wave packets that comprise the CTP. Composite CTP indices, based on the jet index, are shown in Figs. 3c and 3d.

Focusing on the signature of the eastward propagating wave packets, which are indicated by thick solid lines in Figs. 3c and d, there are two noteworthy features. First, statistically

significant CTP wave packets are found in EOF2 (from  $\approx$  lag -9 days to  $\approx$  lag +5 days, and then from lag +12 to lag +14 days for the positive jet phase; from  $\approx$  lag -9 days to  $\approx$  lag +8 days for the negative jet phase). The signal is weaker in EOF1 which shows a statistically significant CTP wave packet only from lag -2 days to lag +6 days for the positive jet phase, while a corresponding wave packet is essentially absent for the negative jet phase. Overall, it can be seen that the CTP wave packet is present over most of the globe, and that their presence is consistent with the visual impression from Figs. 3b and 3i. Similar CTP-like features were also observed by Watanabe (2004) at positive lag days for NAO events, particularly during the months of January and February.

Second, the EOF2-CTP indices take on a negative sign for the positive jet phase, and a positive sign for the negative jet phase. These sign characteristics of the EOF2-CTP have implications for a possible linkage between the CTP and the occurrence of convection over the Indian and western Pacific Oceans. Figure 3b shows that during the negative phase of the EOF2-CTP, the upper tropospheric meridional wind is southward over the northwest Pacific Ocean, while its direction is northward over the eastern Indian Ocean. This meridional wind field corresponds to an anomalous high centered over eastern Asia. Such a wind field has been shown to coincide with an equatorward cold surge (Chang and Lau 1982), and to the excitation of local convection over warm tropical oceans (Kiladis and Weickmann 1992; Hsu et al. 1990). From this perspective, the negative phase of the EOF2-CTP may be expected to excite convection only over the western Pacific, and not over the eastern Indian Ocean. On the same token, for the positive phase of the EOF2-CTP, with its enhanced northerlies centered over India, convection can be triggered farther to the south over the Indian Ocean. Therefore, we can infer that positive jet events may lead to enhanced convection over the

western Pacific Ocean, while negative jet events would tend to excite convection over the Indian Ocean.

## 5. Tropical convection over the Indian and western Pacific Oceans

As discussed in the introduction, previous studies (Cassou 2008; Lin et al. 2009; Lin and Brunet 2011) suggested that there are interactions between tropical convection over the Indian and western Pacific Oceans and the atmospheric circulation over North Atlantic. Our results in Section 4 suggest that the CTP may be involved in this interaction. To further test the relationship between the jet variability and tropical convection, we perform lagged composites of the jet and CTP indices based on the IO and WP precipitation indices (see subsection 2d).

To examine the relationship between tropical convective precipitation and other quantities, we define WP and IO events following the same selection criteria as the jet events (subsection 2b). The selection procedure resulted in 39 IO and 43 WP events. Figure 5 shows the lagged composite map of convective precipitation for the IO and WP indices. For both sets of composites, the convective precipitation starts to rapidly increase at lag -5 days. Figure 5a (at lag 0 days) shows that convective precipitation reaches its maximum over the Indian Ocean and is essentially zero over the western Pacific. This structure conforms to the definition of the IO spatial pattern (see the description in subsection 2d). Similarly, the lag 0 day composites in Fig. 5b displays intensified convection over the western Pacific and very

little convection over the Indian Ocean. The convective precipitation decreases with time at positive lag days in both composite sets.

*a. The jet variability polarity and the convective precipitation patterns*

The relationship between the jet variability and the precipitation patterns are quantified by compositing the jet index based on both the IO and WP indices (see Fig. 6). For the IO index (Fig. 6a), statistically significant positive values above the 90% and 95% confidence levels appear between lag +20 and lag +28 days, indicating that a positive jet event follows an IO event. (For Fig. 6, we slightly relax the definition of a jet event, as described in subsection 2b, and regard a jet event as corresponding to 4 or more consecutive lag days for which the composite jet index is statistically significant.) Moreover, statistically significant negative jet index values are observed between lag -27 and -18 days, indicating that IO events tend to follow negative jet events. For the WP-based composite, the opposite features are observed. This finding suggests that the IO and WP indices are linked to the jet variability through the following relationships:

- Negative jet events are followed by IO events, and this in turn leads to positive jet events.
- Positive jet events lead WP events which are then followed by negative jet events.

Because there are quality issues with ERA-40 convective precipitation data, we also generate precipitation indices with Climate-Prediction-Center Merged Analysis of Precipitation (CMAP) winter data for 1980 through 2002. (The CMAP data coverage begins in 1979.) Because the CMAP data is available in pentad format, to obtain a daily version of the data, a Matlab cubic spline interpolation was used. The IO and WP indices from the CMAP

dataset were generated with the same method as that for the ERA-40 dataset. The correlations between these two datasets are 0.80 and 0.77 for the IO and WP indices, respectively. We illustrate in Figs. 6b and 6c the jet index composites based on the ERA-40 and the CMAP precipitation indices. To facilitate a fair comparison, both sets of composites are constructed for the overlapping period of 1980 to 2002. Although the two composites are variant in terms of time lags and the amplitude, both datasets show that IO events follow negative jet events and lead positive jet events, while the positive jet events lead WP events, and are then followed by negative jet events. Therefore, we conclude that the relationships highlighted by the above bullet points are likely to be robust.

*b. The CTP and the convective precipitation patterns*

The relationship between tropical convection and the CTP is illustrated with lagged composites Fig. 7. In the same manner as in Fig. 3, solid lines are indicated in Fig. 7 to represent features of wave packet propagation. The ‘positive jet’ and ‘negative jet’ are also labeled in this figure, based on the results shown in Fig. 6. This analysis also reveals that the CTP wave pattern is associated with both precipitation indices, at positive and negative lags. For instance, in the WP composite (Fig. 7b), a statistically significant EOF2-CTP wave pattern is seen spanning the North Pacific through to the North Atlantic between lag -18 days and lag -10 days. Then between lag +14 days and lag +23 days, another CTP wave pattern of opposite sign appears over the same region. Similarly in Fig. 7a, it can be seen that there are statistically significant fluctuations in the EOF2-CTP wave pattern associated Indian Ocean convection.

## 6. Interdecadal variability of the jet index

As discussed in the introduction, the results of Hoerling et al. (2004) and Selten et al. (2004) link the interdecadal upward trend in the NAO index to a warming of the tropical Indian Ocean. Motivated by their results, in this section we will examine if there is corresponding interdecadal trend in the jet index, and if so, whether (1) the trend results from an increase and/or decrease in the frequency of intraseasonal positive and negative jet events, respectively, and (2) whether the trend is related to changes in the frequency of intraseasonal convective precipitation events as measured by the IO and WP indices. This connection between interdecadal and intraseasonal variability is motivated by the findings of Lee et al. (2011) who find that the interdecadal trend in both tropical convective precipitation and middle and high latitude upper tropospheric streamfunction anomalies is realized through changes in the frequency distribution of the continuum of intraseasonal convective precipitation and upper tropospheric streamfunction teleconnection patterns (see also Johnson et al. 2008; Johnson and Feldstein 2010; Luo et al. 2007, 2011), each of which fluctuates at a period of 6 to 8 days. Figures 8a and 8b, respectively, show the original (with the interannual variability retained) and the intraseasonal (with the interannual variability removed) jet index time series. The dashed lines are the linear trends based on the least square fitting. While an upward trend toward the positive polarity can be discerned for the original jet index, closely matching intraseasonal time scale fluctuations can be seen in both time series. Using the same selection criteria as described in subsection 2b, except with the interannual variability retained, we found 17 positive and 21 negative events during 1958-1979 (P1), while there were 21 positive and 13 negative events during 1980-2001 (P2). (The sensitivity to choice of

years for P1 and P2 was also evaluated. It was found that if P1 corresponds to 1958-1977 and P2 to 1982-2001, there are 16 positive and 17 negative jet events in P1 and 19 positive and 11 negative jet events in P2. If P1 corresponds to 1958-1974 and P2 to 1985-2001, there are 11 positive and 16 negative jet events in P1 and 17 positive and 10 negative jet events in P2.) To examine whether the upward trend in the jet index is in part due to this shift toward a greater number of positive jet events and a smaller number of negative jet events in P2, relative to P1, we set the jet index equal to zero for all jet events, and then re-calculate the linear trend. If we define an event as extending from lag -15 to lag +15 days, as described in subsection 2c, a 78.2% decrease in the linear trend was found. If an event is defined by a smaller number of days, e.g., from lag -10 to lag +10 days, the decrease in the linear trend is 62.8%. Such results suggest that the answer to question (1) is yes, that the interdecadal change in the frequency of jet events does indeed make an important contribution to the interdecadal trend of the jet index.

To address question (2), we first calculate the frequency of IO and WP events in P1 and P2. It is found that in P1 there are 15 IO and 21 WP events, and in P2 there are 23 IO and 22 WP events. (In order that the number of years within P1 and P2 match, the year 2002 is not included in this calculation. As a result, one IO event within that year is discarded.) This corresponds to a 53.3% increase in the frequency of IO events and a 4.8% increase in the frequency of WP events. Referring back to Fig. 6, based on composites of the jet index associated with IO events, it was shown that negative jet events lead IO events and positive jet events lag IO events. WP events showed the opposite characteristics relative to the jet events. Such calculations focused on the value of the jet index during intraseasonal convective precipitation events. To investigate the tropical convection during jet events,

we perform the reverse calculation, i.e., we calculate composites of the IO and WP indices based on positive and negative jet events (not shown). The results indicate statistically significant values of the IO and WP indices above the 95% confidence level prior to positive and negative jet events, respectively. In contrast, for positive lags, the IO and WP index values were found to exceed just the 90% significance level, for a relatively small number of days. These results indicate that the jet events are more closely linked with tropical convection that precedes the events than with tropical convection that follows the events. As a result, the larger number of positive jet events in P2 compared to P1, may be interpreted as being caused, in part, by the greater frequency of Indian Ocean convective precipitation events during the latter time period. An interpretation for the smaller number of negative jet events in P2 is more challenging, because the frequency of WP events during P2 did not decline. However, we note that the increase in the frequency of IO events from P1 to P2 was an order of magnitude greater than for WP events, and that the excitation of positive jet events by Indian Ocean convection likely coincides with the suppression of negative jet events (a reduction in the frequency of negative NAO events was observed to follow MJO convection over the Indian Ocean (Cassou 2008; Lin et al. 2009; Vitart and Molteni 2010)). Thus, one possible explanation is that the much greater increase in the number of IO events, relative to WP events, also accounts for the smaller number of negative jet events within P2. With regard to the interdecadal upward trend in the jet index, these results suggest, although at this point no more than speculative, that an important contribution may be due to an increase in the frequency of intraseasonal events of tropical Indian Ocean convection.

## 7. Summary and Conclusions

This study examines jet stream variability over the North Atlantic during the boreal winter. This variability is represented by the North Atlantic jet index, which we defined as the first EOF of the zonal wind on seven different vertical levels over the North Atlantic. When the jet index is positive (negative), the tropospheric zonal wind takes on a double (single) jet structure. A pattern correlation calculation (Fig. 2) indicates that the jet index more accurately describes the North Atlantic jet variability than does the NAO index.

We also investigated the relationship between North Atlantic jet variability and tropical convective precipitation on intraseasonal time scales. Two indices were used to measure the intensity of tropical convective precipitation, one for the Indian Ocean (the IO index), and the other for the western Pacific Ocean (the WP index). Composites of the jet index, during intraseasonal convective precipitation events, reveal the following statistically significant intraseasonal time scale relationships:

1. Negative jet events lead the IO events;
2. Positive jet events lag IO events;
3. Positive jet events lead the WP events;
4. Negative jet events lag WP events.

These results are also consistent with the findings of Cassou (2008) and Lin et al. (2009) who showed similar lag/lead relationships between the NAO and MJO. It is important to note that the occurrence of many NAO events, and presumably jet events too, are likely unrelated to tropical convection. This viewpoint is implied by the findings of Cassou (2008) and Lin et al. (2009), which show that the MJO alters the frequency of NAO events, and

that both positive and negative NAO events do coincide with MJO events of all phases.

This study shows evidence that the above intraseasonal relationships are in part manifested through the circumglobal teleconnection pattern (CTP) (Branstator 2002). Feldstein and Dayan (2008) later found that the CTP can be interpreted as corresponding to the time average of intraseasonal time-scale circumglobal wave packets. After utilizing CTP indices which indicate the presence and intensity of the circumglobal wave packets at different longitudes, it was found that the CTP is involved in all four of the above relationships. More specifically, relationships 1 and 3 are linked through the circumglobal wave packet over Asia, and relationships 2 and 4 are connected through the circumglobal wave packet over the North Pacific and North America. In this regard, our interpretation of the physical processes that are responsible for the above four relationships is different from that of Lin et al. (2009) who speculated that the NAO influences the MJO through its excitation of westerly wind anomalies over equatorial Africa and the Indian Ocean.

Our analysis also revealed that the CTP indices are negative during positive jet events and vice versa for negative jet events. If cold air surges play a role in exciting the convection over the two tropical oceans, this sign pairing is consistent with the mechanism. In fact, Kiladis and Weickmann (1992) showed that convection over the equatorial Indian Ocean is preceded by the presence of wave packets in the subtropics. Further support for a relation between cold surges, circumglobal wave packets, and the NAO has been shown in previous studies. For example, Gong et al. (2001) and Jeong and Ho (2005) found that east Asian cold surges overlap with the negative NAO phase, and Chen et al. (2004) showed that these cold surges are associated with wave packets that closely resemble the CTP.

The results of this study also suggest a possible link between intraseasonal variability

in tropical convection and the interdecadal trend of the North Atlantic jet. It was first shown that the interdecadal trend in the jet could be accounted for, to a large extent, by the interdecadal change in the frequency of positive and negative jet events. Then, because relationships 2 and 4 were found to be particularly robust during jet events, and since the increase from P1 to P2 in the number of IO events was much greater than that for WP events, it was suggested that the large increase in the number of intraseasonal convective precipitation events over the Indian Ocean may make an important contribution to this trend.

*Acknowledgments.*

This research was supported by the Chinese NSF grant 40875027, Chinese Scholarship Council, Ph.D. Programs Foundation of the Ministry of Education of China Grant 200800010026 and by National Science Foundation Grants ATM-0649512, ATM-0852379, ATM-0647776, and AGS-1036858 and the National Oceanic and Atmospheric Administration grant NA10OAR4310251. We would like to thank Dr. Nathaniel C. Johnson, Dr. Tingting Gong and Changyun Yoo for offering beneficial comments. We also thank the European Centre for Medium-Range Weather Forecasts (ECMWF) for providing us with the ERA-40 reanalysis data, and the Climate Analysis Branch of the NOAA Earth System Research Laboratory/Physical Sciences Division for providing us with the CMAP precipitation data. In addition, we would like to thank the NOAA Climate Prediction Center for providing us with the climate indices.

## REFERENCES

- Athanasiadis, P. J. and J. M. Wallace, 2010: Patterns of wintertime jet stream variability and their relation to the Storm Tracks. *J. Atmos. Sci.*, **67**, 1361–1381.
- Bader, J. and M. Latif, 2005: North Atlantic Oscillation response to anomalous Indian Ocean sst in a coupled GCM. *J. Climate*, **18**, 5382–5389.
- Benedict, J. J., S. Lee, and S. B. Feildtein, 2004: Synoptic view of the North Atlantic Oscillation. *J. Atmos. Sci.*, **61**, 121–144.
- Branstator, G., 2002: Circumglobal teleconnections, the jet stream waveguide, and the North Atlantic Oscillation. *J. Climate*, **15**, 1893–1910.
- Cassou, C., 2008: Intraseasonal interaction between the Madden-Julian Oscillation and the North Atlantic Oscillation. *Nature*, **455**, 523–527.
- Chang, C. P. and K. M. Lau, 1982: Short-term planetary-scale interactions over the tropics and midlatitudes during northern winter. Part I: Contrasts between active and inactive periods. *Mon. Wea. Rev.*, **110**, 933–946.
- Chen, T. C., W. R. Huang, and J. H. Yoon, 2004: Interannual variation of the east Asian cold surge activity. *J. Climate*, **17**, 401–412.
- Cohen, J. and M. Barlow, 2005: The NAO, the AO and Global Warming: How closely related? *J. Climate*, **18**, 4498–4513.

- Eichelberger, S. J. and D. L. Hartmann, 2007: Zonal jet structure and the leading mode of variability. *J. Climate*, **20**, 5149–5163.
- Feldstein, S. B., 2000: Teleconnections and ENSO: The timescale, power spectra, and climate noise properties. *J. Climate*, **13**, 4430–4440.
- Feldstein, S. B. and U. Dayan, 2008: Circumglobal teleconnections and wave packets associated with Israeli winter precipitation. *Quart. J. Roy. Meteorol. Soc.*, **134**, 455–467.
- Gong, D. Y., S. W. Wang, and J. H. Zhu, 2001: East Asian winter monsoon and Arctic Oscillation. *Geophys. Res. Lett.*, **28**, 2073–2076.
- Hoerling, M. P., J. W. Hurrell, and T. Xu, 2001: Tropical origins for recent North Atlantic climate change. *Science*, **292**, 90–92.
- Hoerling, M. P., J. W. Hurrell, T. Xu, G. T. Bates, and A. S. Phillips, 2004: Twentieth century North Atlantic climate change. Part II: Understanding the effect of Indian Ocean warming. *Clim. Dyn.*, **23**, 391–405.
- Hsu, H., B. J. Hoskins, and F. Jin, 1990: The 1985/86 intraseasonal oscillation and the role of the extratropics. *J. Atmos. Sci.*, **47**, 823–839.
- Hurrell, J. W., 1995: Decadal trends in the North Atlantic Oscillation regional temperatures and precipitation. *Science*, **269**, 676–679.
- Hurrell, J. W. and H. V. Loon, 1997: Decadal variations associated with the North Atlantic Oscillation. *Climatic Change*, **36**, 301–326.

- Jeong, J. H. and C. H. Ho, 2005: Changes in occurrence of cold surges over east Asia in association with Arctic Oscillation. *Geophys. Res. Lett.*, **32**, doi:10.1029/2005GL023024.
- Johnson, N. C. and S. B. Feldstein, 2010: The continuum of North Pacific sea level pressure patterns: Intraseasonal, interannual, and interdecadal variability. *J. Climate*, **23**, 851–867.
- Johnson, N. C., S. B. Feldstein, and B. Tremblay, 2008: The continuum of Northern Hemisphere teleconnection patterns and a description of the NAO shift with the use of Self-Organizing Maps. *J. Climate*, **21**, 6354–6371.
- Kiladis, G. N. and K. M. Weickmann, 1992: Circulation anomalies associated with tropical convection during northern winter. *Mon. Wea. Rev.*, **120**, 1900–1923.
- Lee, S. and S. B. Feldstein, 1996: Mechanism of zonal index evolution in a two-layer model. *J. Atmos. Sci.*, **53**, 2232–2246.
- L’Heureux, M. L. and R. W. Higgins, 2007: Boreal winter links between the Madden-Julian Oscillation and the Arctic Oscillation. *J. Climate*, **21**, 3040–3050.
- Li, S., M. P. Hoerling, and S. Peng, 2006: Coupled ocean-atmosphere response to Indian Ocean warmth. *Geophys. Res. Lett.*, **33**, doi:10.1029/2005GL025558.
- Lin, H. and G. Brunet, 2011: Impact of the North Atlantic Oscillation on the forecast skill of the Madden-Julian Oscillation. *Geophys. Res. Lett.*, **38**, doi:10.1029/2010GL046131.
- Lin, H., G. Brunet, and J. Derome, 2009: An observed connection between the North Atlantic Oscillation and the Madden-Julian Oscillation. *J. Climate*, **22**, 364–380.

- Lorenz, D. J. and D. L. Hartmann, 2003: Eddy-zonal flow feedback in the Northern Hemisphere winter. *J. Climate*, **16**, 1212–1227.
- Luo, D., Y. Diao, and S. B. Feldstein, 2011: The variability of the Atlantic storm track and the North Atlantic Oscillation: A link between intraseasonal and interannual variability. *J. Atmos. Sci.*, **68**, 577–601.
- Luo, D., T. Gong, and Y. Diao, 2007: Dynamics of eddy-driven low-frequency dipole modes. Part iii: Meridional displacement of westerly jet anomalies during two phases of NAO. *J. Atmos. Sci.*, **64**, 3232–3248.
- Matthews, A. J., 2008: Primary and successive events in the Madden-Julian Oscillation. *Quart. J. Roy. Met. Soc.*, **134**, 439–453.
- Matthews, A. J. and G. N. Kiladis, 1999: The tropical-extratropical interaction between high-frequency transients and the Madden-Julian Oscillation. *Mon. Wea. Rev.*, **127**, 661–677.
- Palmer, T. N., 1988: Large-scale tropical,extratropical interactions on time-scales of a few days to a season. *Aust. Met. Mag.*, **36**, 107–125.
- Robinson, W. A., 1993: Mechanisms of low-frequency variability in a simple model with orography. *J. Atmos. Sci.*, **50**, 878–888.
- Selten, F. K., G. W. Branstator, H. A. Dijkstra, and M. Kliphuis, 2004: Tropical origins for recent and future Northern Hemisphere climate change. *Geophys. Res. Lett.*, **31**, doi: 10.1029/2004GL020739.

- Semenov, V. A., M. Latif, J. H. Jungclauss, and W. Park, 2008: Is the observed NAO variability during the instrumental record unusual? *Geophys. Res. Lett.*, **35**, doi:10.1029/2008GL033273.
- Uppala, S. M., P. W. Kallberg, and Co-authors, 2005: The ERA-40 reanalysis. *Quart. J. Roy. Met. Soc.*, **131**, 2961–3012.
- van Loon, H. and J. C. Rogers, 1978: The seesaw in winter temperatures between Greenland and Northern Europe. Part I: General description. *Mon. Wea. Rev.*, **106**, 296–310.
- Vitart, F. and F. Molteni, 2010: Simulation of the Madden-Julian Oscillation and its teleconnections in the ECMWF forecast system. *Quart. J. Roy. Met. Soc.*, **136**, 842–855.
- Wallace, J. M. and D. S. Gutzler, 1981: Teleconnections in the geopotential height field during the Northern Hemisphere winter. *Mon. Wea. Rev.*, **109**, 784–812.
- Watanabe, M., 2004: Asian jet waveguide and a downstream extension of the North Atlantic Oscillation. *J. Climate*, **17**, 4674–4691.
- Wittman, M. A. H., A. J. Charlton, and L. M. Polvani, 2005: Notes and correspondence on the meridional structure of annular modes. *J. Climate*, **18**, 2119–2122.
- Woollings, T., A. Hannachi, and B. Hoskins, 2010: Variability of the North Atlantic eddy-driven jet stream. *Quart. J. Roy. Met. Soc.*, **136**, 856–868.
- Yu, J. and D. L. Hartmann, 1993: Zonal flow vacillation and eddy forcing in a simple GCM of the atmosphere. *J. Atmos. Sci.*, **50**, 3244–3259.

Zhou, S. and A. Miller, 2005: The interaction of the Madden-Julian Oscillation and the Arctic Oscillation. *J. Climate*, **18**, 143–159.

## List of Figures

- 1 The spatial structure of the North Atlantic jet variability leading mode (EOF1).  
(a) The horizontal cross-section at 250 hPa and (b) the vertical cross-section at 30°W. 33
- 2 Histogram of the pattern correlation coefficient. The upper panel is the correlation between the actual zonal wind field and the jet variability pattern for (a) the positive polarity; (b) the negative polarity. The middle panel is the correlation between the 500-hPa geopotential height field and the NAO (500-hPa) loading pattern for (c) the positive polarity; (d) the negative polarity. The lower panel is the correlation between the actual 250-hPa zonal wind field and the NAO loading pattern for the 250-hPa zonal wind for (e) the positive polarity; (f) the negative polarity. Please see the text for additional detail. 34
- 3 The EOF1 (a) and EOF2 (b) of the 300-hPa nondivergent meridional wind. The numbers mark the ten extrema of the corresponding ten circumglobal wave packet indices. Composite circumglobal wave packet index values for (c) EOF1 and EOF2 for positive jet events; (d) EOF1 and EOF2 for negative jet events; The abscissa marks the circumglobal wave packet indices and the ordinate indicates the time-lag. The solid lines denote positive values and dashed lines negative values. The zero contour is omitted. Shading indicates values that are statistically significant above the 95 % confidence level for a two-sided *t*-test. The sloping line segments indicate the peak of the circumglobal wave packet indices. 35

- 4 Composite of the 250-hPa streamfunction based on the jet index during December-February of 1958–2002. The left column is for positive phase composite at lag days -13, -9, -5, 0, 5, 12. The right column is the same as the left column except for the negative phase composite. The solid lines represent positive values and the dashed lines negative values. The contour interval is  $1.5 \times 10^6 m^2 s^{-1}$ . The zero contour is omitted. Shading indicates values that exceed the 95% confidence level for a two-sided  $t$ -test. 36
- 5 Composites of convective precipitation (with interannual variability and the seasonal cycle removed) based on (a) IO; (b) WP. The solid lines represent positive values and dashed lines negative values. The contour interval is  $1.0 \times 10^{-3}$  m. The zero contour is omitted. The Monte Carlo method is used to compute statistical significance. Shading indicates values that are statistically significant above the 95 % confidence level. 37
- 6 Lagged composite map of the jet index based on exclusive convective precipitation indices of ERA-40 data during (a) 1958–2002 and (b) 1980–2002. (c)Lagged composite map of the jet index based on exclusive convective precipitation indices of CMAP data during 1980–2002. See text for detail. The solid line represents composite values based on IO and the dashed line composite values based on WP. The asterisks and open circles indicate those points which are statistically significant above the 95% and 90% confidence levels, respectively. 38

- 7 Lagged composite map of the circumglobal teleconnection wave pattern indices in EOF1 and EOF2 based on (a) IO; (b) WP. Both interannual variability and the seasonal cycle have been removed. Solid lines denote the composite of jet index based on IO events, and dashed lines denote that based on WP events. The abscissa marks the circumglobal wave packet indices and the ordinate indicates the time-lag. Solid lines denote positive values and dashed lines negative values. The zero contour is omitted. Shading indicates values that are statistically significant above the 90 % confidence level. The sloping line segments indicate the peak of the circumglobal wave packet indices. The ‘positive jet’ denotes positive jet events and ‘negative jet’ for negative jet events. 39
- 8 The original jet index (a) and the detrended jet index(b). The dashed lines indicate the linear trends of the curves. 40

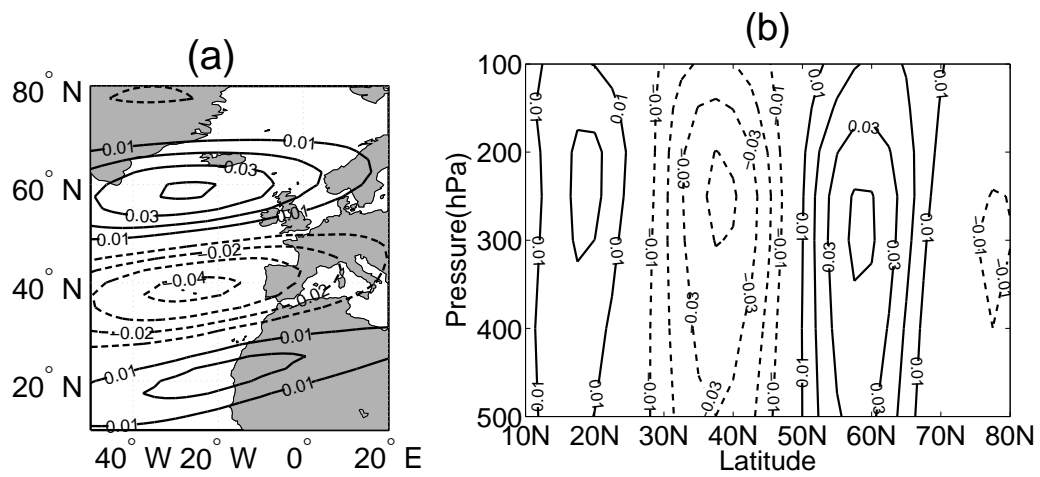


FIG. 1. The spatial structure of the North Atlantic jet variability leading mode (EOF1). (a) The horizontal cross-section at 250 hPa and (b) the vertical cross-section at 30°W.

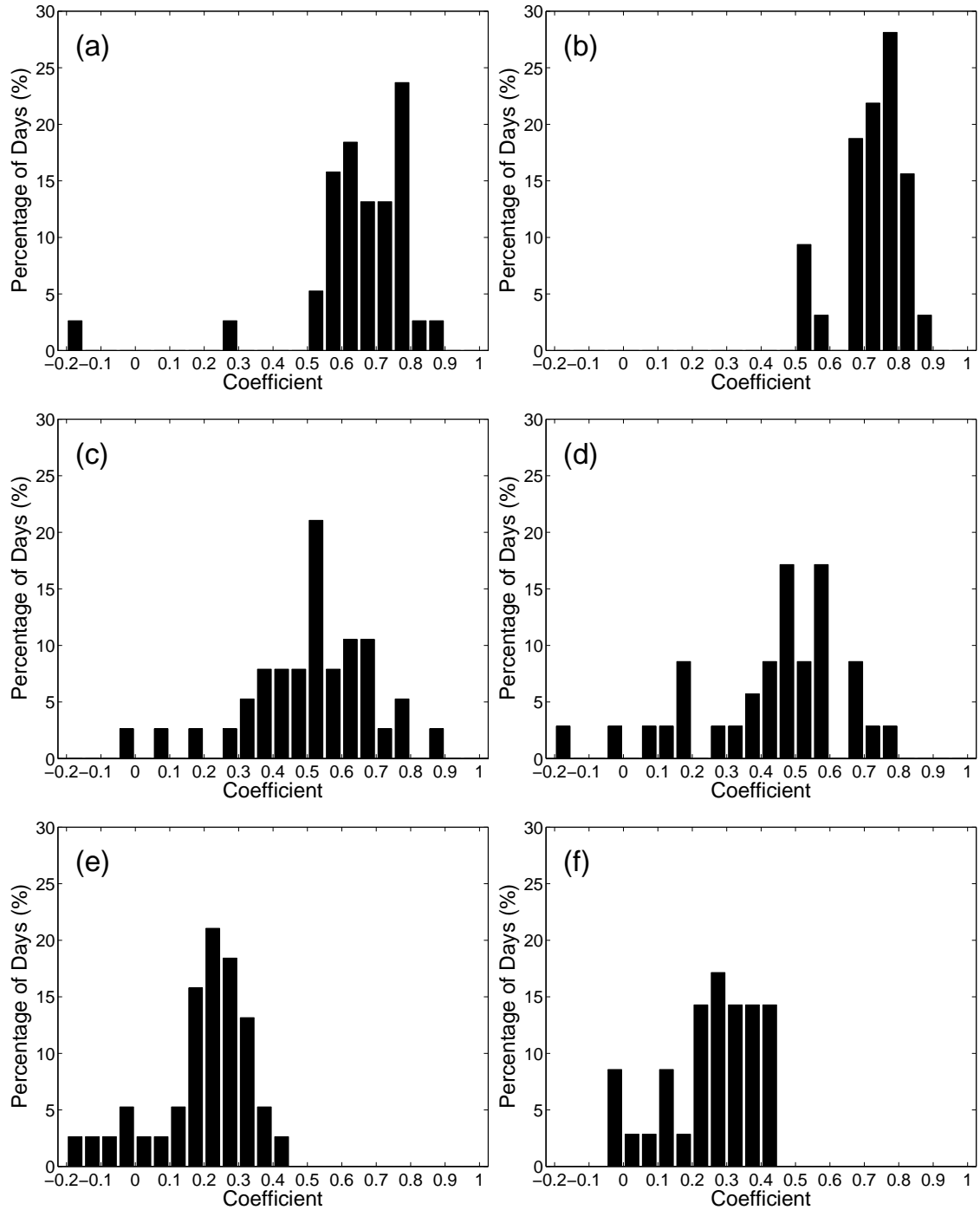


FIG. 2. Histogram of the pattern correlation coefficient. The upper panel is the correlation between the actual zonal wind field and the jet variability pattern for (a) the positive polarity; (b) the negative polarity. The middle panel is the correlation between the 500-hPa geopotential height field and the NAO (500-hPa) loading pattern for (c) the positive polarity; (d) the negative polarity. The lower panel is the correlation between the actual 250-hPa zonal wind field and the NAO loading pattern for the 250-hPa zonal wind for (e) the positive polarity; (f) the negative polarity. Please see the text for additional detail.

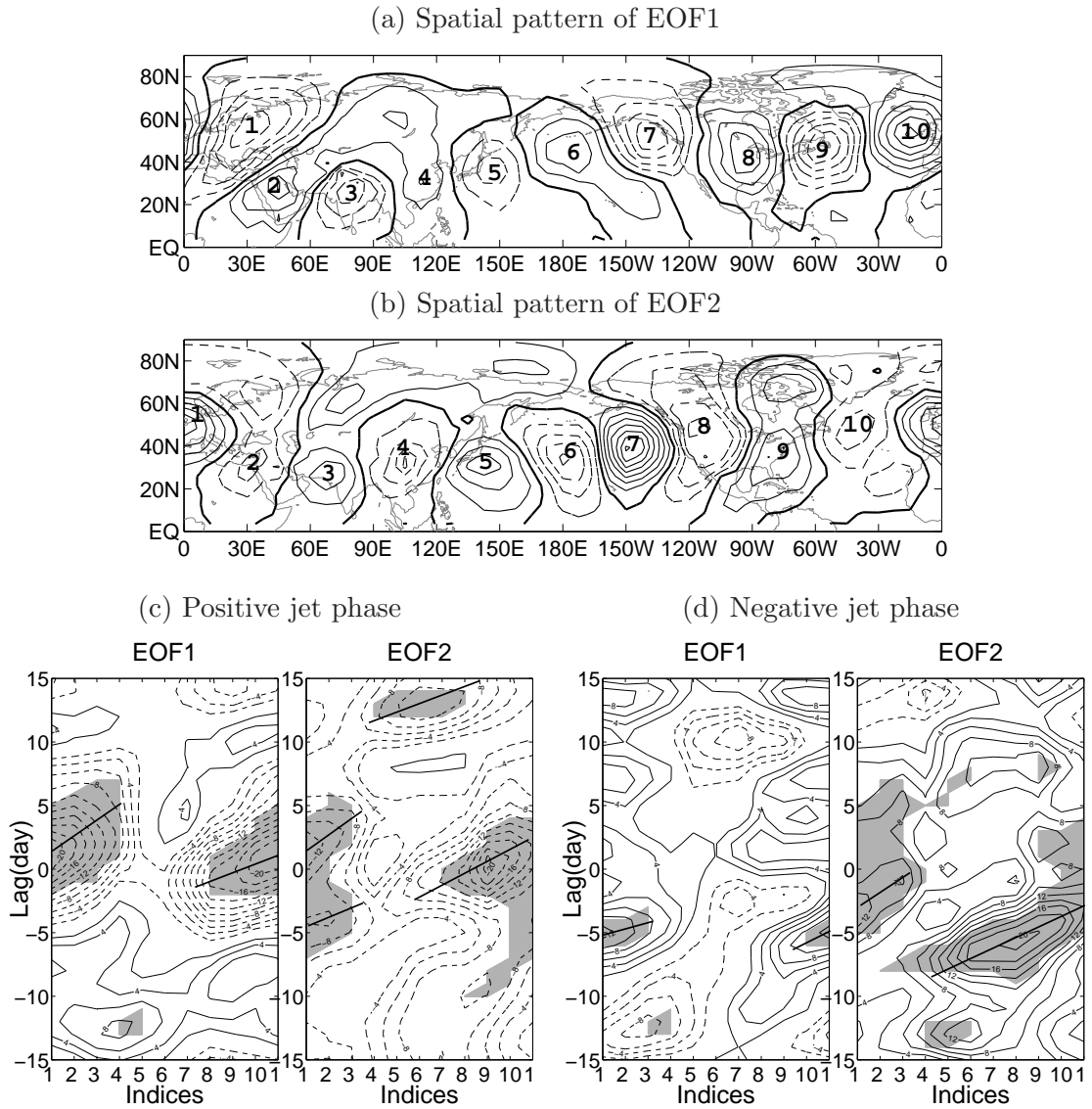


FIG. 3. The EOF1 (a) and EOF2 (b) of the 300-hPa nondivergent meridional wind. The numbers mark the ten extrema of the corresponding ten circumglobal wave packet indices. Composite circumglobal wave packet index values for (c) EOF1 and EOF2 for positive jet events; (d) EOF1 and EOF2 for negative jet events; The abscissa marks the circumglobal wave packet indices and the ordinate indicates the time-lag. The solid lines denote positive values and dashed lines negative values. The zero contour is omitted. Shading indicates values that are statistically significant above the 95 % confidence level for a two-sided  $t$ -test. The sloping line segments indicate the peak of the circumglobal wave packet indices.

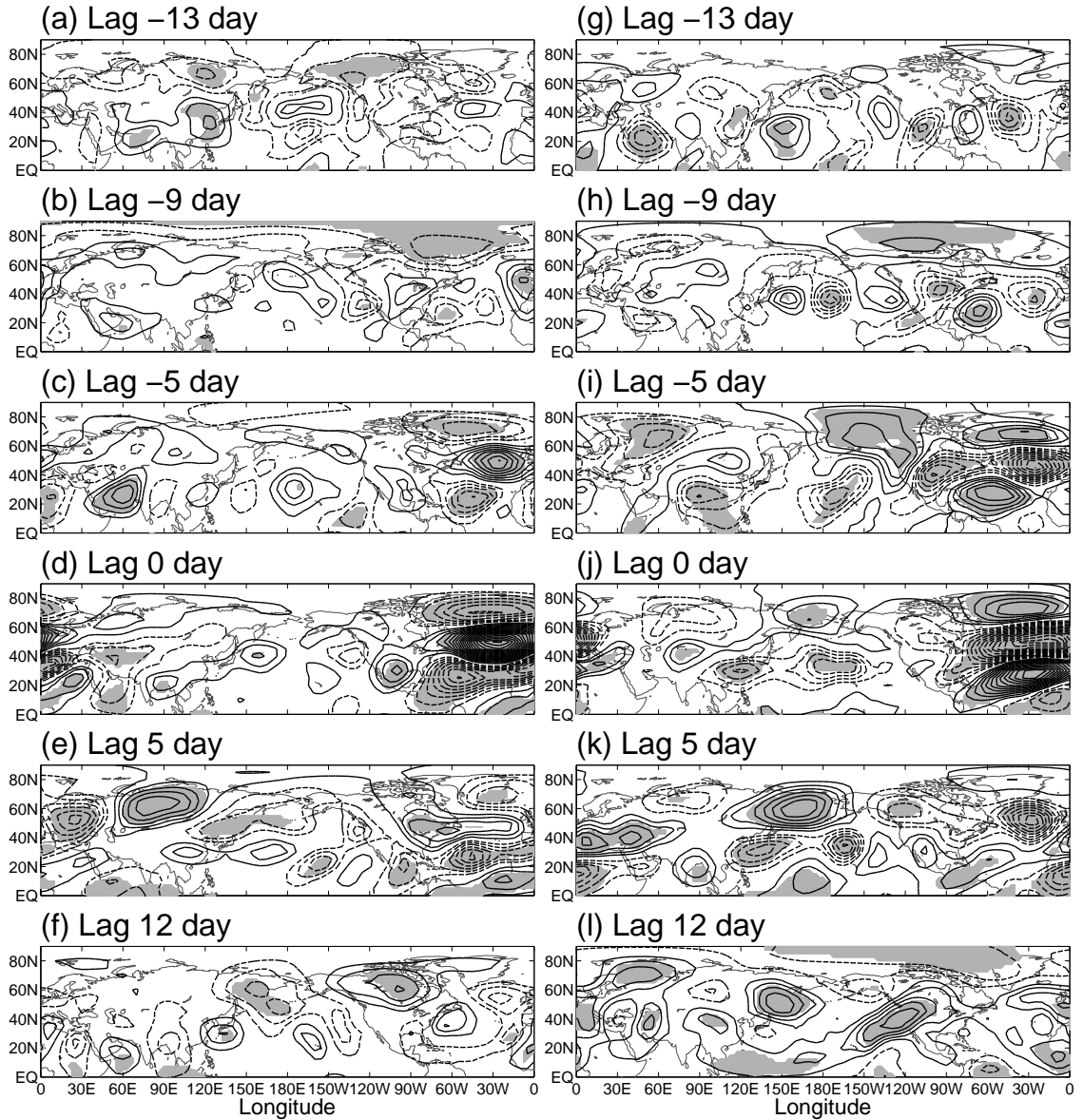


FIG. 4. Composite of the 250-hPa streamfunction based on the jet index during December-February of 1958–2002. The left column is for positive phase composite at lag days -13, -9, -5, 0, 5, 12. The right column is the same as the left column except for the negative phase composite. The solid lines represent positive values and the dashed lines negative values. The contour interval is  $1.5 \times 10^6 m^2 s^{-1}$ . The zero contour is omitted. Shading indicates values that exceed the 95% confidence level for a two-sided  $t$ -test.

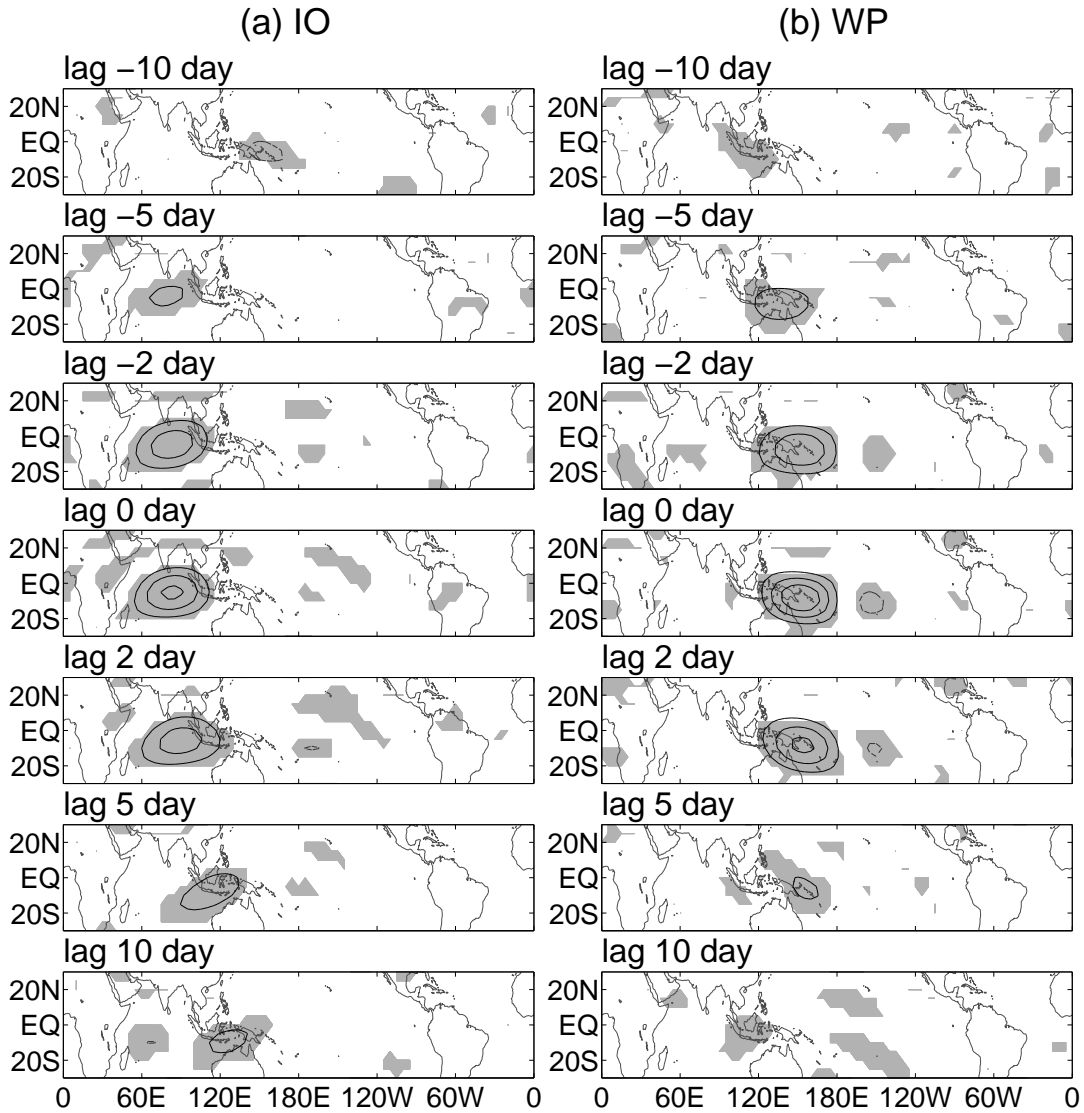


FIG. 5. Composites of convective precipitation (with interannual variability and the seasonal cycle removed) based on (a) IO; (b) WP. The solid lines represent positive values and dashed lines negative values. The contour interval is  $1.0 \times 10^{-3}$  m. The zero contour is omitted. The Monte Carlo method is used to compute statistical significance. Shading indicates values that are statistically significant above the 95 % confidence level.

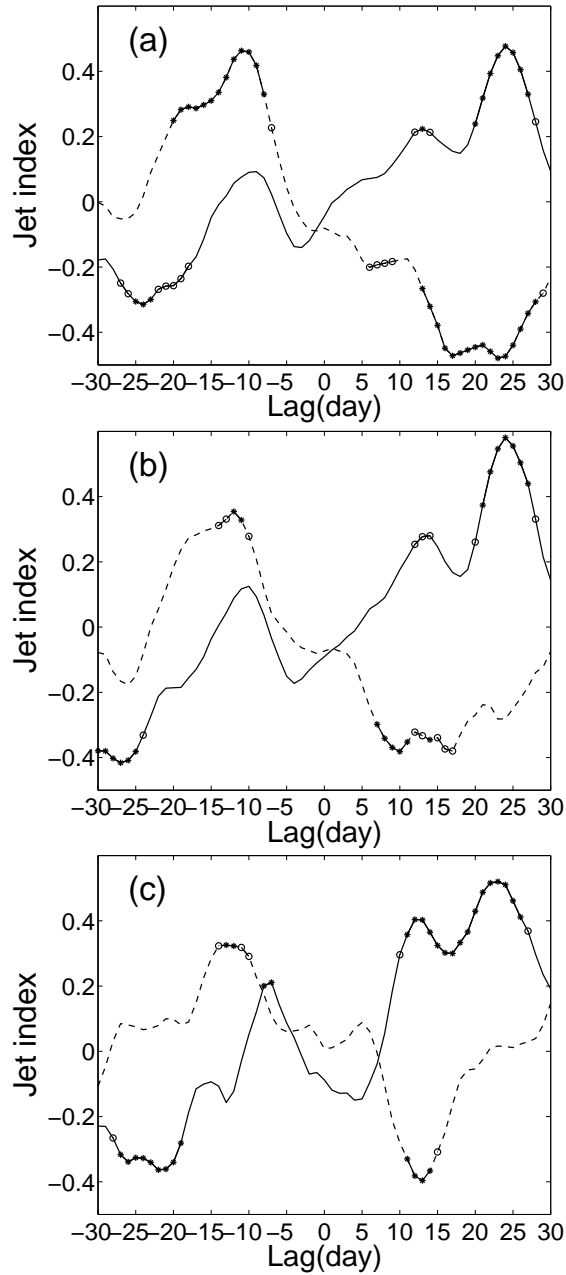


FIG. 6. Lagged composite map of the jet index based on exclusive convective precipitation indices of ERA-40 data during (a) 1958–2002 and (b) 1980–2002. (c) Lagged composite map of the jet index based on exclusive convective precipitation indices of CMAP data during 1980–2002. See text for detail. The solid line represents composite values based on IO and the dashed line composite values based on WP. The asterisks and open circles indicate those points which are statistically significant above the 95% and 90% confidence levels, respectively.

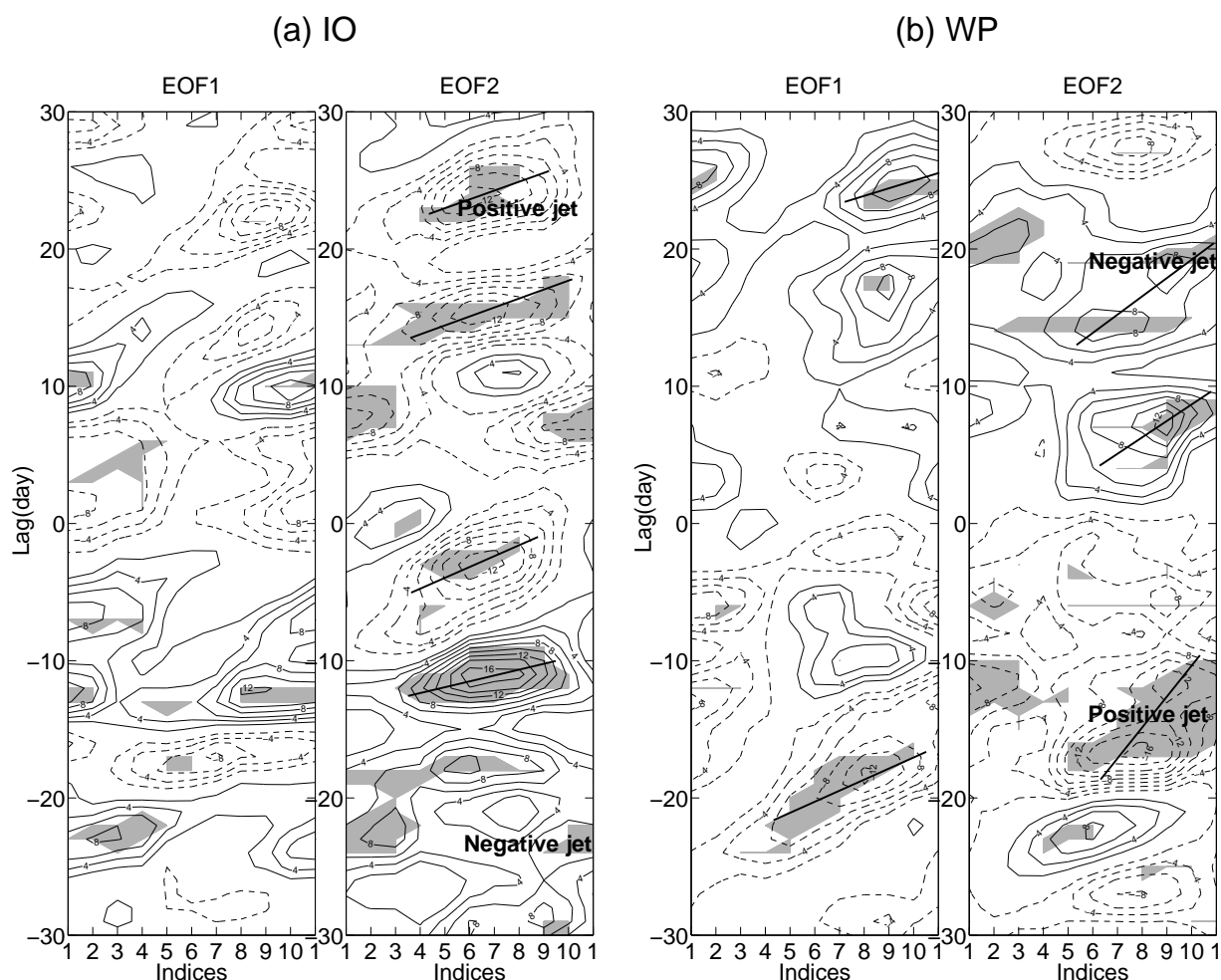


FIG. 7. Lagged composite map of the circumglobal teleconnection wave pattern indices in EOF1 and EOF2 based on (a) IO; (b) WP. Both interannual variability and the seasonal cycle have been removed. Solid lines denote the composite of jet index based on IO events, and dashed lines denote that based on WP events. The abscissa marks the circumglobal wave packet indices and the ordinate indicates the time-lag. Solid lines denote positive values and dashed lines negative values. The zero contour is omitted. Shading indicates values that are statistically significant above the 90 % confidence level. The sloping line segments indicate the peak of the circumglobal wave packet indices. The ‘positive jet’ denotes positive jet events and ‘negative jet’ for negative jet events.

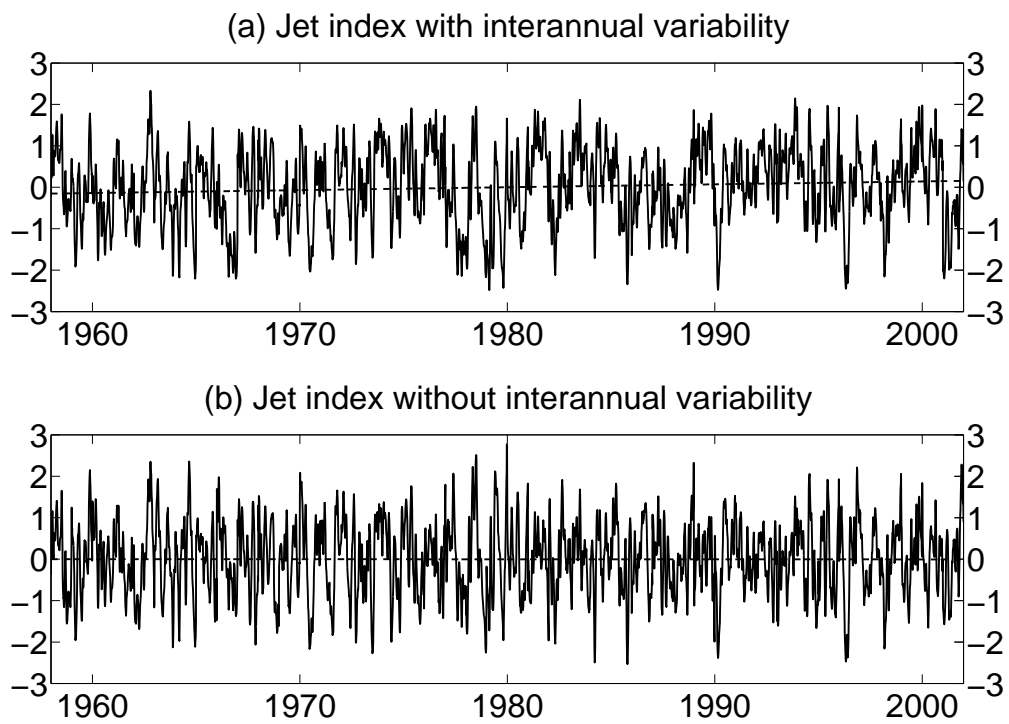


FIG. 8. The original jet index (a) and the detrended jet index(b). The dashed lines indicate the linear trends of the curves.